IOP Publishing New J. Phys. 27 (2025) 013010 https://doi.org/10.1088/1367-2630/ada4d0

New Journal of Physics
The open access journal at the forefront of physics

Deutsche Physikalische Gesellschaft DPG
IOP Institute of Physics

Published in partnership with: Deutsche Physikalische Gesellschaft and the Institute of Physics

OPEN ACCESS

RECEIVED
25 August 2024

REVISED
28 November 2024

ACCEPTED FOR PUBLICATION
2 January 2025

PUBLISHED
21 January 2025

PAPER

Multi-pulse Fourier codes for bit transmission at the quantum limit

Matteo Rosati

Dipartimento di Ingegneria Civile, Informatica e delle Tecnologie Aeronautiche, Universitá Roma Tre, Via Vito Volterra 62, I-00146 Rome, Italy

E-mail: matteo.rosati@uniroma3.it

Keywords: quantum communication, optical communication, joint-detection-receiver, quantum advantage, quantum information processing

Abstract

Bit-transmission can be enhanced by the use of quantum detection techniques, realizing a joint-detection receiver (JDR) that is able to decode transmitted signals via a collective operation and achieve the Holevo channel capacity. Explicit JDR designs proposed so far employ the Hadamard or Fourier transform to perform a phase-to-intensity translation of the information encoding, effectively falling in the class of on-off-keying (OOK) modulation techniques; they improve over classical decoders but fall short of the Holevo capacity, particularly at large signal mean photon number $n \gtrsim 1$. Here we introduce new families of decoders based on multi-pulse and multi-level codes. We compute the rate of these codes exactly, and provide a comprehensive study of their performance. We show that multi-pulse codes can approach the rate of OOK closely, providing a simplified design for quantum-enhanced communication in the photon-starved regime; furthermore, multi-level codes can approach generalized-OOK strategies with multiple pulse types, thus they can be employed in the larger photon-number regime.

1. Introduction

Quantum information theory aims at establishing the ultimate limits of information-processing tasks, based on a quantum-mechanical description of the employed physical systems. In communication, Holevo [1] established a seminal theorem that determines the maximum amount of bits transmittable on a quantum channel, i.e. the classical capacity of said channel, encompassing the use of quantum correlations among multiple signals both at the encoding and decoding stage. More recently, it was shown that the class of phase-insensitive bosonic quantum Gaussian channels, modelling the effects of loss, additive noise, and amplification in optical-fiber and free-space communication via continuous-variable optical quantum systems, does not require entanglement at the encoding stage [2, 3]. However, to the best of our knowledge, a decoder achieving the Holevo capacity still requires an optimal joint-detection receiver (JDR), that analyses the received signals in a coherent and collective way [4–16]. Despite much work on the subject, only few sub-optimal designs of JDR have been proposed to date, based either on discrete transforms (DTs), e.g. Hadamard and Fourier [17–20], or on general linear-optical interactions [16]. Furthermore, these designs perform well only in the regime where the number of received photons is small ($n \lesssim 1$).

One common feature of the DT-JDR designs is that the information is initially encoded into the phases of a sequence of coherent-states of the electromagnetic field, keeping the mean-photon-number constant for each symbol in the sequence, and ensuring that different messages are encoded into sequences that are orthogonal in phase-space. The decoder performs a DT on the signal sequences aimed at translating the phase-modulation into an intensity-modulation; in this way, different messages are identified by the presence of a single pulse in a different symbol position, easily read-out via photo-detection. From this perspective, DT schemes can be seen as a sub-class of on-off-keying (OOK) ones, characterized by the transmission of iid symbols, each of which can be either vacuum, with high probability, or a high-photon-number pulse, with low probability. Indeed, by optimizing the pulse probability it is always possible to outperform DT via OOK.

On the other hand, the general linear-optical schemes discovered in [16] took a step beyond the single-pulse regime, producing sequences where multiple pulses of different mean-photon-numbers can be

detected after the decoding operation. Such schemes surpass the communication rate of DT ones in the region of $0.1 \lesssim n \lesssim 1$ photons. Unfortunately, given the numerical nature of [16], it is difficult to extrapolate a systematic coding/decoding method from there.

In light of these reasons, here we introduce multi-pulse and multi-level codes based on the Fourier transform, in an effort to take the best of both JDR design methods known to date. The rationale behind our new codes is that, thanks to the linearity of the decoding operations in phase-space, one can combine signal sequences corresponding to different messages, giving rise to new sequences after decoding, which contain multiple pulses with potentially different mean photon number levels. Multi-pulse sequences effectively realize a higher-order approximation of sequences generated by iid repetitions of OOK, while multi-level ones can in principle approximate generalizations of OOK using more than one pulse type. The latter are also known to provide an optimal modulation for the classical discrete-time Poisson channel capacity [21, 22], which can be related to the quantum channels under study via the photo-detection process [23, 24].

Finally, while here we show the approximate equivalence of complex multi-symbol JDR schemes with simpler single-symbol OOK ones (see also [10]), we stress that the use of JDR techniques is nevertheless favorable in communication scenarios where a peak-energy constraint is present. This is a motivated assumption in most practical settings, e.g. due to effective limits to the maximum power that can be produced and/or that the transmission medium can support before the onset of capacity-limiting effects, or due to the use of low-brightness signals for security purposes.

2. Bit-transmission at the quantum limit

We consider a bit-transmission protocol that encodes information on M modes of the electromagnetic field. For the purpose of describing the protocol and computing its rate, for simplicity we make the assumption that the modes have fixed frequency ν, and hence they are either time- or spatially- separated; nevertheless, our results are equally applicable to frequency-separated modes. We describe the signal as a quantum-mechanical state of the field: each mode is supported on an infinite-dimensional Hilbert space $\mathcal{H}_i$ and the corresponding field amplitude can be written in terms of the photon-creation and -annihilation operators $a_i, a_i^\dagger$, which obey the bosonic commutation relations $[a_i, a_j^\dagger] = \delta_{i,j}1$. The mean number of photons is $n^{\rm in}$ for each signal $i = 1, \cdots, M$. The communication line is modelled by a pure-loss bosonic quantum Gaussian channel, characterized by its attenuation coefficient τ; hence, the received signal photon number and energy per mode is given by $n = \tau\, n^{\rm in}$. Since there is no added noise, without loss of generality in the rest of the article we employ the received mean-number of photons n as independent variable, rather than the input one. We also note that our results are equally applicable to other phase-insensitive channels, including effects of additive-noise and amplification.

For bit-transmission on a phase-insensitive Gaussian channel with a mean photon-number constraint n, the optimal encoding employs iid coherent states $|\alpha_i\rangle_i = D(\alpha_i)|0\rangle_i$, whose two quadrature mean-values $x_i = \sqrt{2}\,{\rm Re}\alpha_i$ and $p_i = \sqrt{2}\,{\rm Im}\alpha_i$ are chosen from a Gaussian distribution, like in classical communication [2, 25]. Here, the ket $|0\rangle$ represents the vacuum state of the field, while

$$D(\alpha) = \exp\left(-\alpha a^\dagger - \alpha^* a\right) \tag{1}$$

is an optical displacement operator with complex mean-value $\alpha \in \mathbb{C}$. Using the optimal encoding and performing heterodyne detection on each mode at the receiver, the resulting number of bits transmitted per channel use is given by the Shannon capacity of the additive-white-Gaussian-noise channel with[1]

$$C_{\rm sh} = \log(1+n), \tag{2}$$

where a 1-photon-noise contribution is present due to the shot-noise limited detection process. On the other hand, Holevo [1] provided a capacity formula that is optimized over all potential receivers, including those employing quantum processing to improve the detection process. In particular, for a Gaussian modulation we have

$$C_{\rm ho} = g(n) = (n+1)\log(n+1) - n\log n. \tag{3}$$

It is well-known [25] that $C_{\rm ho} \geqslant C_{\rm sh}$, and the advantage is particularly evident for long transmission distance, where the received signal carries few or even less than one photon on average, or in the medium distance in the presence of amplification [26].

[1] Throughout the text we use base-2 logarithms.

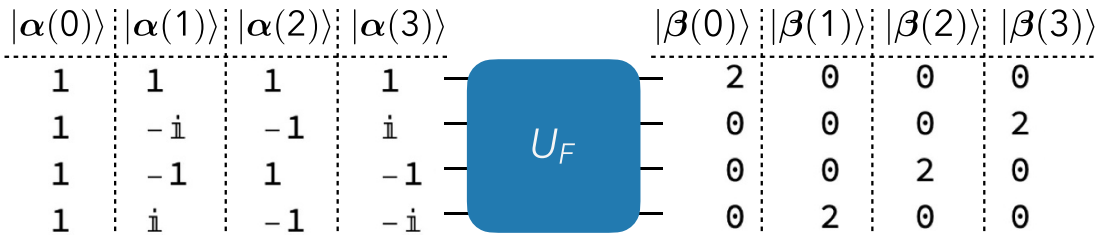

Figure 1. Depiction of the FM scheme for $M = 4$ and $n = 1$. the transmitted codewords are shown in the columns on the left, with the ith entry corresponding to the coherent-state complex amplitude on the ith mode. After applying the optical Fourier DT, the codewords are mapped to those on the right.

In the setting of low received photon number and zero added noise, that we consider here, the Gaussian modulation can be substituted with a simpler binary-phase-shift-keying (BPSK) modulation. At the receiver, the signal can take two equiprobable values, $\alpha_i = \pm\sqrt{E}$ and, employing the best quantum single-symbol detector, i.e. the Dolinar detector achieving the Helstrom bound for these two states [27–29], we obtain a rate

$$R_{\rm hel}^{\rm bpsk} = 1 - H_2\left(\frac{1+\sqrt{1-e^{-4n}}}{2}\right). \tag{4}$$

Thus, unlocking the advantage predicted by Holevo (3) requires the design of a quantum receiver, that is capable of processing multiple symbols at once and extract collective information about the transmitted sequence.

In [17], the Green–Hadamard machine (GHM) was proposed, relying on a linear-optical implementation of the Hadamard DT to encode and decode the message, followed by threshold photo-detection. Importantly, the GHM outperforms single-symbol receivers such as (4) at received mean photon number $n \lesssim 0.1$.

Finally, let us note that, in the low-received-photon-number region one is interested to transmit a large number of bits per received photon. This is encapsulated by the photon-information-efficiency (PIE), which can be computed for a generic capacity or rate R as

$$\mathrm{PIE} = \frac{R}{n}. \tag{5}$$

2.1. Fourier protocol and its relation with OOK

In [17], the GHM was proposed, relying on a linear-optical implementation of the Hadamard DT of order $M = 2^i$ to encode and decode the message, followed by threshold photo-detection. In [20], a similar Fourier machine (FM) based on the Fourier DT was proposed; We will base our multi-pulse and multi-level codes on the FM, as it works for any integer order M, allowing more freedom for the code parameters. Hence, here we briefly sum up the protocol based on FM (an example of which is shown in figure 1).

For any positive integer $M \in \mathbb{N}$ let $F^{(M)}$ be a Fourier matrix of elements

$$F_{j\ell}^{(M)} = \frac{1}{\sqrt{M}}\omega^{j\cdot\ell}, \tag{6}$$

with $\omega = \exp(-\mathrm{i}2\pi/M)$ the Mth root of unity; for ease of notation, we omit the index M when clear from the context. The linear-optical Fourier DT of order M is represented by a unitary operator U_F that acts on a coherent-state sequence as

$$U_F|\boldsymbol{\alpha}\rangle = |F\boldsymbol{\alpha}\rangle, \tag{7}$$

where $\boldsymbol{\alpha} \in \mathbb{C}^M$ and $|\boldsymbol{\alpha}\rangle = \bigotimes_{i=0}^{M-1}|\alpha_i\rangle_i$. The unitary U_F can be decomposed into basic beam-splitter and phase-shift gates as a general multi-port interferometer via standard methods [30–33]. The code then consists of M inverse-Fourier coherent-state sequences of mean photon number n

$$\mathcal{C} = \left\{|\boldsymbol{\alpha}(j)\rangle : \boldsymbol{\alpha}_i(j) = \omega^{-i\cdot j}\sqrt{n},\ \forall i,j = 0,\cdots,M-1\right\}. \tag{8}$$

The Fourier decoder then applies the Fourier DT to the received codeword $|\boldsymbol{\alpha}(j)\rangle$, mapping it to an output codeword $|\boldsymbol{\beta}(j)\rangle = U_F|\boldsymbol{\alpha}(j)\rangle$ such that

$$\beta_i(j) = \sum_{\ell=0}^{M-1} F_{i\ell}\alpha_\ell(j) = \frac{1}{\sqrt{M}}\sum_{\ell=0}^{M-1}\omega^{\ell(i-j)}\sqrt{n} = \delta_{ij}\sqrt{Mn}, \tag{9}$$

i.e. after the Fourier DT the codewords are in the format of a pulse-position-modulation, with a single pulse having M times more photons than the transmitted pulses, placed in one of M possible positions in the sequence. This conversion of phase-to-intensity information makes the single high-photon-number pulse more distinguishable from the vacuum, increasing the photodetector's effective sensitivity in settings with low received photon number. Indeed, in the absence of background or detection noise, the unpopulated positions will never produce a photocount, whereas the probability of detecting one or more photons from the populated position, and hence correctly identifying the codeword, is

$$p_0 = 1 - e^{-Mn}. \tag{10}$$

The resulting rate using soft-decoding on the photodetection outcomes is

$$R_{\rm fm} = \frac{1}{M}\left[h\left(1-p_0\right) + M\cdot h\left(\frac{p_0}{M}\right) - H_2\left(p_0\right)\right] = \frac{\log M}{M}p_0, \tag{11}$$

where we have defined $h(x) = -x\log x$ and used the property $h(x\cdot y) = xh(y) + yh(x)$. Observe that this coincides with the rate of a GHM but, unlike the latter, it is valid for any $M \in \mathbb{N}$.

On the other hand, we note that, if one employs an OOK modulation with symbols $\mathcal{C}_{\rm ook} = \{|0\rangle, |\sqrt{n/q}\rangle\}$ and respective probabilities $\{1-q, q\}$, followed by photodetection, the ensuing communication rate is

$$R_{\rm ook} = H_2\left(q\left(1-e^{-\frac{n}{q}}\right)\right) - qH_2\left(1-e^{-\frac{n}{q}}\right) \tag{12}$$

$$= \left(1-e^{-\frac{n}{q}}\right)\cdot h\left(q\right) + h\left(1-q\left(1-\cdot e^{-\frac{n}{q}}\right)\right) - n\cdot e^{-\frac{n}{q}}. \tag{13}$$

In the following, we refer to this strategy as a q-OOK protocol. In particular, setting $q = 1/M$ we obtain

$$R_{\rm ook}\Big|_{q=\frac{1}{M}} = R_{\rm fm} + h\left(1-\frac{p_0}{M}\right) - n\left(1-p_0\right), \tag{14}$$

and, defining the difference $\Delta R(n) = R_{\rm ook}|_{1/M} - R_{\rm fm}$, we find that its derivative is positive:

$$\Delta R'\left(n\right) \propto \log\left(1-\frac{p_0}{M}\right) + n = \frac{1}{M}\log\left(1-\frac{p_0}{M}\right)^M + n \geqslant \frac{1}{M}\log\left(1-p_0\right) + n = 0, \tag{15}$$

where we have used that $(1-x)^c \geqslant 1-cx$ for $x \in [0,1]$, following from Lagrange's second-order remainder. Hence we conclude that $\Delta R(n)$ is an increasing function of n, with the difference between FM and $1/M$-OOK being small at small photon number and attaining its maximum at large photon number, i.e.

$$\max_n \Delta R\left(n\right) = \lim_{n\to\infty}\Delta R\left(n\right) = h\left(1-\frac{1}{M}\right). \tag{16}$$

This is evidence that the GHM and FM are a first-order approximation to OOK in the regime of small n and M. Indeed, if we take M iid repetitions of OOK with $q = 1/M$, the resulting sequences will have on average one pulse of mean-photon-number Mn, i.e. matching the codewords at the output of a FM machine of order M.

3. Multi-pulse Fourier protocol

The previous observations motivate us to ask whether there exist other codes that, after decoding, generate output codewords with more than one pulse, similarly to the sequences that one can expect from M iid repetitions of OOK with $q > 1/M$.

We consider then a strategy which generates $K \geqslant 1$ pulses in each output codeword of length M, using the same FM described above. This can be done by transmitting codewords whose mean-values correspond to the sum of K single-pulse Fourier codewords of (8):

$$\boldsymbol{\alpha}\left(\mathbf{j}\right) = \frac{1}{\sqrt{K}}\sum_{k=1}^{K}\boldsymbol{\alpha}\left(j_k\right), \tag{17}$$

where we have properly normalized the mean-value in order to respect the mean-photon-number constraint (an example construction is shown in figure 2).

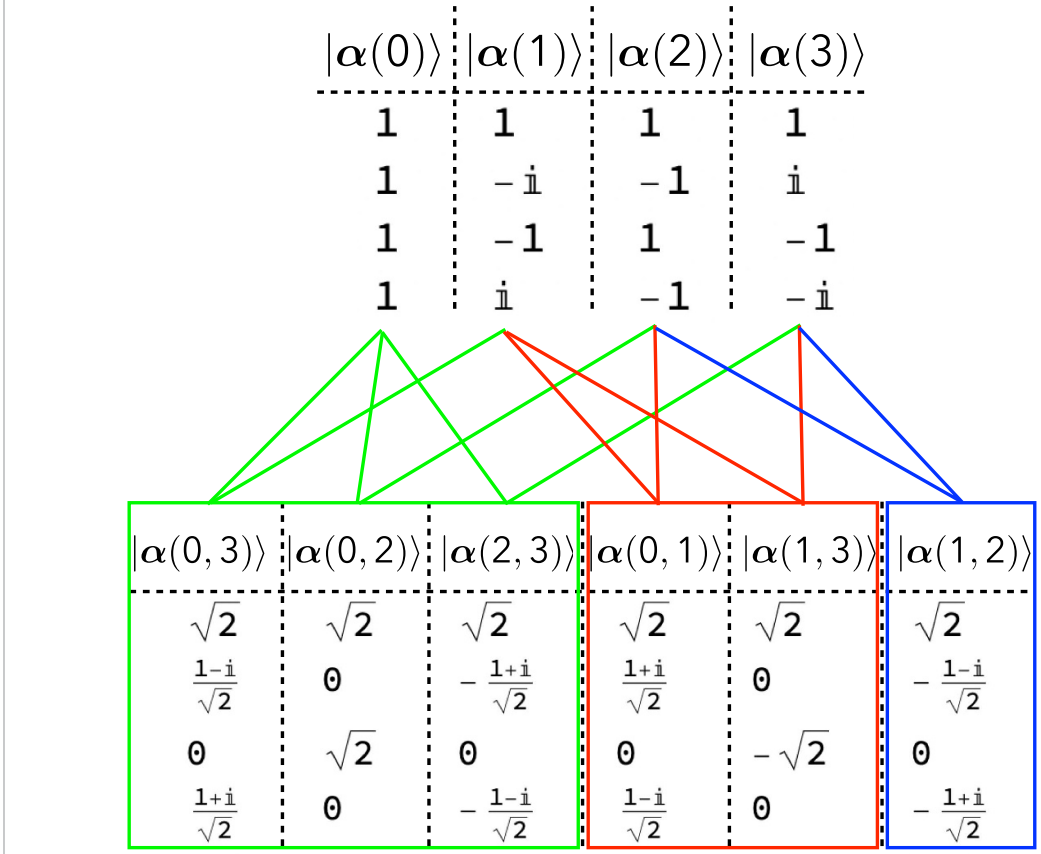

Figure 2. Construction of the multi-pulse FM codewords for $M = 4$, $n = 1$ and $K = 2$ (lower table). These can be obtained by summing the complex amplitudes of K single-pulse codewords (upper table) and properly rescaling by $\sqrt{K}$ in order to respect the mean-photon-number constraint. Each column represents a codeword, with the ith entry corresponding to the coherent-state complex amplitude on the ith mode.

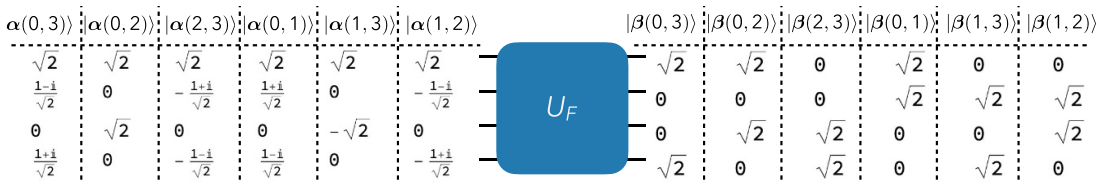

Figure 3. Depiction of the multi-pulse FM protocol for $M = 4$ and $n = 1$. The transmitted codewords are shown in the columns on the left, with the ith entry corresponding to the coherent-state complex amplitude on the ith mode. After applying the optical Fourier DT, the codewords are mapped to those on the right. In practice, the transmitted codewords can be generated at the encoder by preparing the output codewords and applying the inverse Fourier DT $U_F^\dagger$.

Here, the vector $\mathbf{j} \in \{0, \cdots, M-1\}^K$ effectively encodes K distinct positions of the pulses in the state $|\boldsymbol{\beta}(\mathbf{j})\rangle = U_F|\boldsymbol{\alpha}(\mathbf{j})\rangle$ at the output of the decoder:

$$\beta_i(\mathbf{j}) = \frac{1}{\sqrt{K}} \sum_{k=1}^{K} \sum_{\ell=0}^{M-1} F_{i\ell} \alpha_\ell(j_k) = \frac{1}{\sqrt{K}} \sum_{k=1}^{K} \delta_{ij_k} \sqrt{Mn}. \tag{18}$$

The total number of such codewords, i.e. the code-size, is $\binom{M}{K}$ (see figure 3 for a depiction of the protocol).

In this case, in order to compute the soft-decoding rate we need to consider events with $k = 0, \cdots, K$ total clicks, corresponding to how many pulses from the output codeword where correctly detected. The conditional probability of detecting k pulses in specific positions, given any transmitted codeword, is

$$P(k) = p^k \cdot (1-p)^{K-k}, \tag{19}$$

where $p = 1 - e^{-\frac{Mn}{K}}$. If k pulses are detected, these could have come from $\binom{M-k}{K-k}$ different codewords. Therefore, the marginal probability of a k-clicks event is

$$\bar{P}(k) = P(k)\,\frac{\binom{M-k}{K-k}}{\binom{M}{K}}. \tag{20}$$

Furthermore, for each value of k, there are $\binom{M}{k}$ different ways in which they can be distributed among the M positions. The resulting rate then is

$$R_{\mathrm{fm}}(K) = \frac{1}{M}\sum_{k=0}^{K}\binom{M}{k}\cdot\left[h\left(\bar{P}(k)\right) - \frac{\binom{M-k}{K-k}}{\binom{M}{K}}\cdot h\left(P(k)\right)\right] \tag{21}$$

$$= -\frac{1}{M}\sum_{k=0}^{K}\binom{K}{k}\cdot P(k)\cdot\log\frac{\binom{M-k}{K-k}}{\binom{M}{K}} \tag{22}$$

$$= \frac{1}{M}\left[\log\binom{M}{K} - \mathbb{E}_{k\sim\mathrm{Bin}(K,p)}\left[\log\binom{M-k}{K-k}\right]\right], \tag{23}$$

where in the second equality we have used the fact that $\binom{M-k}{K-k}\binom{M}{k} = \binom{K}{k}\binom{M}{K}$, while in the last one we have identified $\binom{K}{k}P(k)$ as the binomial distribution of k successful trials out of K with success probability p, and $\mathbb{E}_{k\sim P}[f(k)]$ is the expectation with respect to the random variable k sampled from P. Note that for $K = 1$ we recover the single-pulse FM rate (11).

3.1. Performance analysis in the low-photon-number regime

For $n \ll 1$ we have $p \simeq Mn/K$ and we can approximate the rate at first order as

$$R_{\mathrm{fm}}(K) \simeq \frac{1}{M}\left[\log\binom{M}{K} - (1-Mn)\log\binom{M}{K} - Mn\log\binom{M-1}{K-1}\right] \tag{24}$$

$$= n\log\frac{\binom{M}{K}}{\binom{M-1}{K-1}} = n\log\frac{M}{K}, \tag{25}$$

which matches OOK in the same limit, provided that we choose $q = K/M$:

$$R_{\mathrm{ook}}\Big|_{q=\frac{K}{M}} \simeq \frac{Mn}{K}\cdot h\left(\frac{K}{M}\right) = n\log\frac{M}{K}. \tag{26}$$

This result is confirmed by figure 4(a), where we plot the FM multi-pulse rate for fixed M and increasing K, and the corresponding K/M-OOK rate. We can observe that, as K increases, the two rates match in a broader range of photon-number values, implying that FM's with larger K make a better approximation of the corresponding OOK rate. Furthermore, while it is clear that for fixed M and $n \ll 1$ the best rate is attained by the standard FM, i.e. $K = 1$, already for $n \gtrsim 0.2$ we observe that the use of a multi-pulse FM, i.e. $K \geqslant 2$, provides an advantage with respect to the standard FM.

On the other hand, we can compare the FM performance with the optimal OOK rate, obtained my maximizing with respect to the pulse probability q. In the low-photon-number region $n \ll 1$, an approximate solution can be found by expanding the rate to second order in n,

$$R_{\mathrm{ook}} \simeq \left(\frac{n}{q} - \frac{1}{2}\left(\frac{n}{q}\right)^2\right)\cdot h(q) + h\left(1 - q\left(\frac{n}{q} - \frac{1}{2}\left(\frac{n}{q}\right)^2\right)\right) - n\left(1 - \frac{n}{q}\right) \tag{27}$$

$$\simeq \left(-n\log q + \frac{n^2}{2}\frac{\log q}{q}\right) + h\left(1 - n + \frac{1}{2}\frac{n^2}{q}\right) - n\left(1 - \frac{n}{q}\right) \tag{28}$$

$$\simeq \left(-n\log q + \frac{n^2}{2}\frac{\log q}{q}\right) + n - \frac{1}{2}\frac{n^2}{q} - \frac{n^2}{2} - n\left(1 - \frac{n}{q}\right) \tag{29}$$

where we used that $h'(1-x) = (\log(1-x)+1)$ and $h''(1-x) = -1/(1-x)$, hence $h(1-x) \simeq x - x^2/2$ for $x \simeq 0$. Setting its first derivative equal to 0 we obtain

$$0 \simeq \frac{n}{q}\left(-1 - \frac{n}{2q}\log q\right) \tag{30}$$

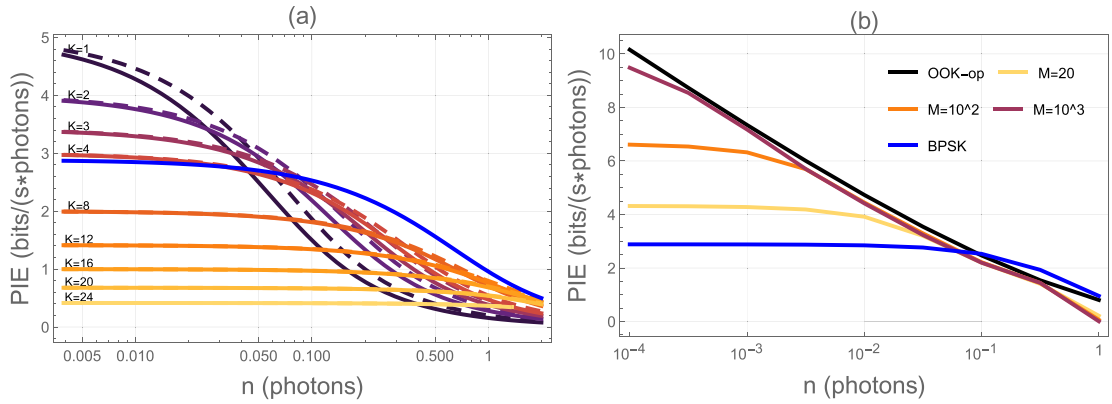

Figure 4. (a) Plot of the multi-pulse FM PIE (23) vs. the mean-photon-number, for a code of order $M = 32$ and varying number of pulses K as shown by the labels (solid lines). The dashed lines represent the PIE of OOK protocols (13) with $q = K/M$, while the blue line is the BPSK PIE (4). (b) Plot of the multi-pulse FM PIE (23) for three values of M and the corresponding optimal $K = [Mq_{\rm op}(n)]$ vs. the mean-photon number n. The black curve corresponds to the numerically optimized OOK PIE, while the blue line is the BPSK PIE (4).

which is solved approximately for $q_{\rm op}(n) = \frac{n}{2}\log\frac{1}{n}$, corresponding to a rate

$$R_{\rm ook}\Big|_{q=q_{\rm op}(n)} \simeq -n\log q_{\rm op}(n) \simeq n\log\frac{2}{n}. \tag{31}$$

In light of the previous considerations (equations (25) and (26)), we can then obtain a multi-pulse FM protocol with rate close to optimal OOK (31) by setting $\frac{K}{M} = q_{\rm op}(n)$. As a consequence, for any K and $n \ll 1$, there exists a FM protocol with K pulses and close-to-optimal rate, provided that its order can be chosen as $M = [K/q_{\rm op}(n)]$. Conversely, for any M and $n \ll 1$, there exists a FM protocol of order M and close-to-optimal rate, provided that it uses $K = [Mq_{\rm op}(n)]$ pulses. Naturally, these values of M, K are subject to the constraints $1 \leqslant K \leqslant M$, which cannot be met for all n.

In light of these reasons we conclude that, in the low-photon-number regime, our multi-pulse FM can be used to simplify the design of communication protocols with respect to the single-pulse one. Indeed, a disadvantage of the single-pulse FM is that it requires to change the order M, hence building a completely different encoder/decoder device, depending on the photon-number n; we recall that the latter depends on the travel distance and input power. On the other hand, one can still attain the optimal rate by fixing a sufficiently large order M and varying K, hence effectively employing a single encoder/decoder device but changing the number of pulses sent through it, depending on n. We provide an illustrative example in figure 4(b), where we plot the FM PIE for various values of M and optimal $K = [Mq_{\rm op}(n)]$; comparing the curves with the optimal OOK PIE, we observe that it is approachable in the entire photon-number region $n \in [3\times10^{-3}, 3\times10^{-1}]$ by, e.g. fixing $M = 100$ and changing the number of pulses K of the protocol, but not the FM device itself.

Finally, we compare the performance of a multi-pulse Fourier code with that of previous JDR's in the literature: (i) the single-pulse JDR's, obtained with our notation for $K = 1$ and $M = 2^i$ (Hadamard [17]) or arbitrary M (Fourier [20]); and (ii) the multi-pulse JDR's with optimal bit-error-rate (BER), obtained via a numerical supervised-learning approach in [16]. The results are shown in figure 5 for $M = 5$, where we also plot the envelope of the best single or two-pulse codes maximized over all possible values of M. We observe that our two-level FM is able to surpass the performance of the best single-pulse FM and approach the BER-optimal JDR in the region where the latter has an advantage. This suggests that the multi-pulse characteristic is crucial to surpass Hadamard-like schemes. Still, we observe that the BER-optimal JDR works with codes of much larger size than that of the single- and two-pulse codes for $M = 5$ (of code-size respectively 5 and 10).

3.2. Performance analysis in the large-photon-number regime

For general n, we can prove that the K/M-OOK rate is not smaller than the FM rate for any $K \geqslant 1$, like in the single-pulse case. Defining the difference $\Delta R(n,K) = R_{\rm ook}|_{q=K/M} - R_{\rm fm}(K)$ and computing its derivative

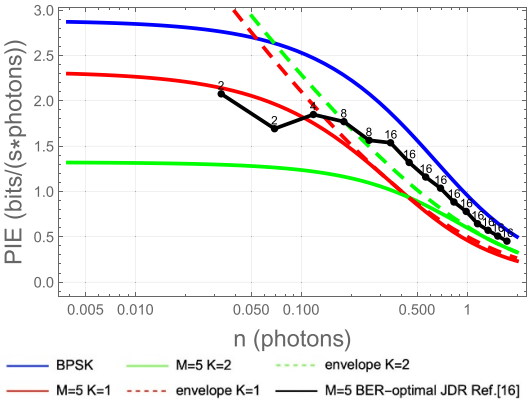

Figure 5. Plot of PIE vs. the mean-photon-number for several protocols on $M = 5$ modes: the two-pulse FM (23) introduced in this paper, the single-pulse FM of [20], and the numerical JDR with optimal bit-error-rate (BER) of [16]. The latter datapoints are labelled with the size of the code employed by the corresponding numerical JDR. The dashed lines represent the envelope of single- and two-pulse FM's with respect to M, and we also plot the single-symbol BPSK rate for reference.

with respect to the photon number we obtain

$$\frac{\mathrm{d}\Delta R(n,K)}{\mathrm{d}n} = p'\left[h\left(\frac{K}{M}\right) + \frac{K}{M}\left(\log\left(1-\frac{K}{M}p\right)\right) + n\right] - (1-p) \tag{32}$$

$$+ \frac{1}{M}\sum_{k=0}^{K}\binom{K}{k}[k\cdot p^{k-1}(1-p)^{K-k} \tag{33}$$

$$+ (K-k)\cdot p^{k}(1-p)^{K-k-1}]\log\binom{M-k}{K-k}. \tag{34}$$

Considering that $p' = (1-p)\frac{M}{K}$ we can gather the positive term $1-p$; furthermore, in the first-term of the sum we can change the index to $t = k-1$, thus identifying both terms as binomials $\mathrm{Bin}(K-1,p)$. Then, up to positive factors the derivative is

$$\frac{\mathrm{d}\Delta R(n,K)}{\mathrm{d}n} \propto \log\left(\frac{M}{K}-p\right) + n + \mathbb{E}_{t\sim\mathrm{Bin}(K-1,p)}\left[\log\frac{K-t}{M-t}\right] \tag{35}$$

$$\geqslant \log\left(\frac{M-p}{K-Kp}\right) - \log\mathbb{E}_{t\sim\mathrm{Bin}(K-1,p)}\left[\frac{M-t}{K-t}\right] = \log\frac{1+\frac{1}{K}\frac{p}{1-p}}{1+\frac{1}{M}\frac{p}{1-p}} \geqslant 0 \tag{36}$$

where in the first inequality we used $n = -\log(1-p)$ and Jensen's inequality for the concave function $\log\frac{M-t}{K-t}$.

Hence we conclude that $\Delta R(n,K)$ is an increasing function of n for all $K \geqslant 1$, with the difference between FM and K/M-OOK being small at small photon number and attaining its maximum at large photon number, i.e.

$$\max_n \Delta R(n,K) = \lim_{n\to\infty}\Delta R(n,K) = H_2\left(\frac{K}{M}\right) - \frac{1}{M}\log\binom{M}{K} \tag{37}$$

showing that the FM and K/M-OOK rate have a gap for large-photon number and finite M, which tends to zero as $M\to\infty$ with K/M finite. Furthermore, it is also clear that, in the large-n limit both rates attain their maximum value at $K = M/2$ and they are symmetric about this point.

This limiting behavior is confirmed in the finite-n regime by numerical evidence. In figure 6(a) we plot the FM rate for all values of $K = 1,\cdots,M-1$, highlighting two facts: (i) the condition of half-filling, i.e. $K = \frac{M}{2}$, is optimal even at finite $n > 1$, and (ii) in the finite-n regime, there is an asymmetry between FM rates at $K < \frac{M}{2}$ and $K > \frac{M}{2}$, with the latter being larger then the former. This might be puzzling at first, since when switching from $\frac{M}{2} - i$ to $\frac{M}{2} + i$, the role of pulses and vacua is simply exchanged; however, note that the probability p is not symmetric under this exchange. The symmetry is recovered asymptotically, where only the first term in (23) matters. In figure 6(b) instead we plot the ratio of the multi-pulse FM and the K/M-OOK rate for optimal $K = M/2$ and increasing M. We observe that the gap between the two rates, present at finite M (37), is slowly reduced, with the ratio saturating to 1 for large M.

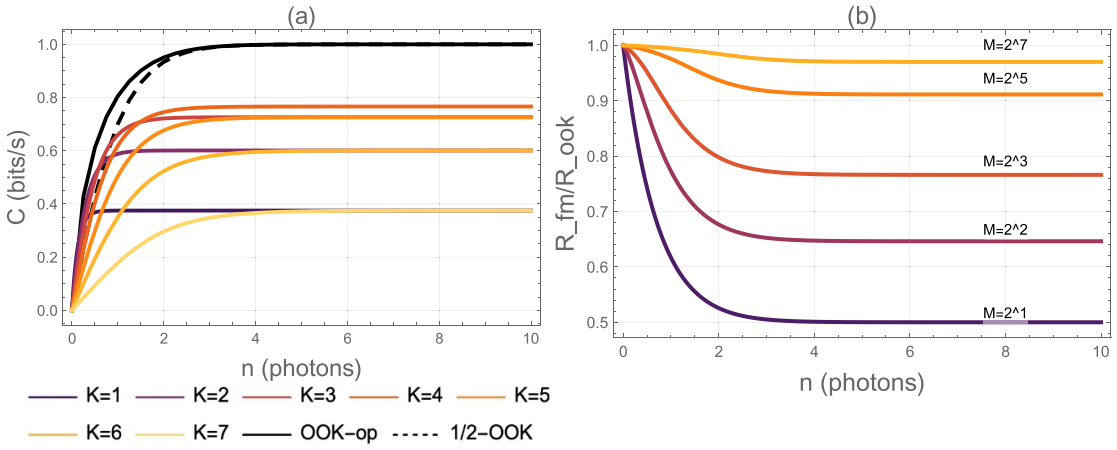

Figure 6. (a) Plot of the multi-pulse FM rate (23) vs. the mean-photon-number for $M = 8$ and all possible K values. The black curves represent the numerically optimized OOK rate (solid) and the $1/2$-OOK rate (dashed). (b) Plot of the ratio between the multi-pulse FM (23) and K/M-OOK rate (13) for the optimal $K = M/2$ and varying M.

Finally, we observe that in the large-n limit the optimal OOK rate is obtained for $q \to 1/2$. In figure 6(a) we also plot the numerically optimized OOK and $1/2$-OOK, showing that the approach to the asymptotically optimal value of q happens quickly when $n > 1$. Interestingly, this limiting value corresponds to that of a multi-pulse FM at half-filling, i.e. $K = M/2$.

4. Multi-level Fourier protocol

In order to surpass the performance of BPSK, it is possible to go beyond OOK and consider a modulation with vacuum and a certain number of pulses of successively higher energy, taking place with successively decreasing probability; for example it is known that a Gamma distribution has good performance for the discrete-time Poisson channel (induced by photon-counting detection on a quantum signal, in our setting) [21, 22]. We consider then a strategy which generates $K = \sum_{t=1}^{T} K_t$ pulses in each output codeword of length M using the FM, with the following property: for each $t = 1, \cdots, T$, the output codeword has exactly K_t pulses of mean-photon-number $\frac{M \cdot n}{T \cdot K_t}$ (an example construction is shown in figure 7).

This can be attained by transmitting a codeword whose mean-value vector corresponds to the sum of T codewords, each with K_t pulses for $t = 1, \cdots, T$;

$$\boldsymbol{\alpha}(\mathbf{j}_1, \cdots, \mathbf{j}_T) = \frac{1}{\sqrt{T}} \sum_{t=1}^{T} \frac{\boldsymbol{\alpha}(\mathbf{j}_t)}{\sqrt{K_t}}, \tag{38}$$

where $\boldsymbol{\alpha}(\mathbf{j}_t)$ is a K_t-pulse codeword (17) and we have properly normalized the mean-value vector to respect the mean-photon-number constraint. Consequently, the FM decodes this input sequence by producing the output codeword $|\boldsymbol{\beta}(\mathbf{j}_1, \cdots, \mathbf{j}_T)\rangle = U_F |\boldsymbol{\alpha}(\mathbf{j}_1, \cdots, \mathbf{j}_T)\rangle$ with

$$\boldsymbol{\beta}(\mathbf{j}_1, \cdots, \mathbf{j}_T) = \frac{1}{\sqrt{T}} \sum_{t=1}^{T} \frac{1}{\sqrt{K_t}} \sum_{k=1}^{K_t} \sum_{\ell=0}^{M-1} F_{i\ell} \alpha_\ell \left(j_{t,k} \right) \tag{39}$$

$$= \frac{1}{\sqrt{T}} \sum_{t=1}^{T} \frac{1}{\sqrt{K_t}} \sum_{k=1}^{K_t} \sum_{\ell=0}^{M-1} \delta_{i, j_{t,k}} \sqrt{Mn}, \tag{40}$$

where, for each $t = 1, \cdots, T$, the vector $\mathbf{j}_t$ encodes the position of t-type pulses in the output codeword. Furthermore, if we define $\mathbf{K} = (K_1, \cdots, K_T, M - K)$ as the vector containing the number of pulses of each type, and the number of vacua, the code-size is given by the multinomial coefficient

$$\binom{M}{\mathbf{K}, M-K} = \frac{M!}{K_1! \cdots, K_T! \, (M-K)!}. \tag{41}$$

Finally, since we are now using more than one pulse type, in order to distinguish them the receiver needs to count photons. Let us then suppose that the receiver uses photon-number-resolving detectors, with resolution up to L photons, i.e. aggregating in the largest outcome all photon-counts larger than or equal to L. Figure 8 shows a depiction of the protocol.

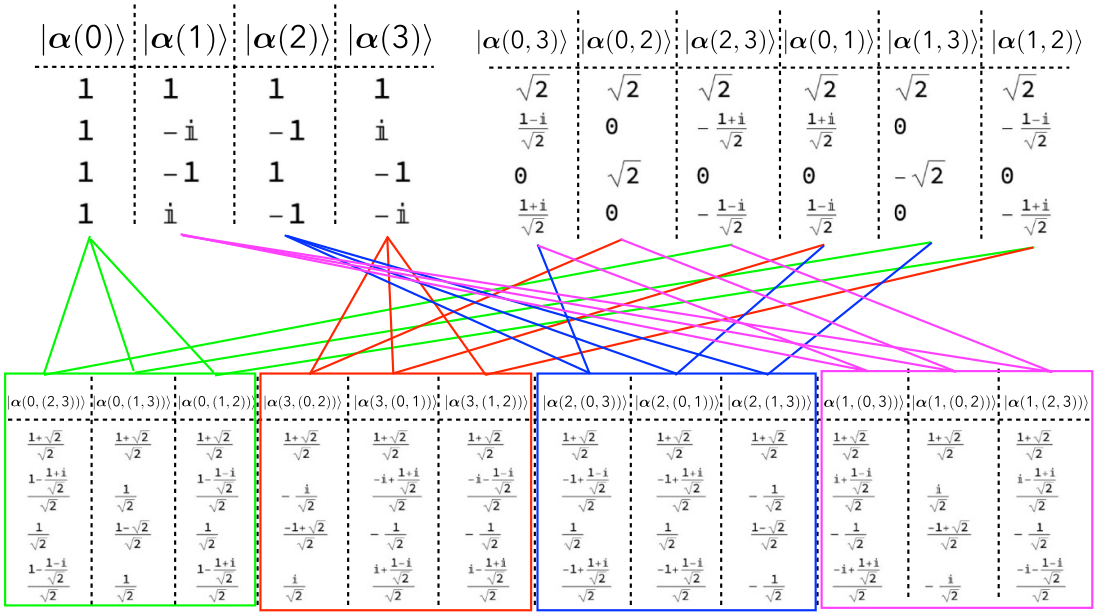

Figure 7. Construction of the multi-level FM codewords for $M=4$, $n=1$ and $\mathbf{K}=(1,2)$ (lower table). These can be obtained by summing the complex amplitudes of a single-pulse codeword (upper left table) with those of a $K_2=2$ multi-pulse codeword (upper right table), each properly rescaled by $\sqrt{K_t}$ in order to respect the mean-photon-number constraint. A further constraint requires that the pulse positions in both original codewords are distinct. Each column represents a codeword, with the ith entry corresponding to the coherent-state complex amplitude on the ith mode.

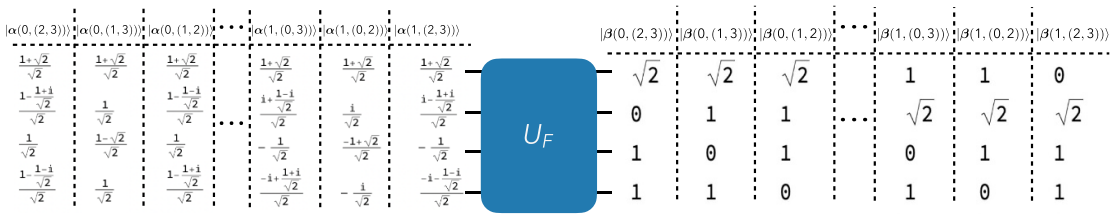

Figure 8. Depiction of the multi-pulse FM protocol for $M=4$, $n=1$ and $\mathbf{K}=(1,2)$. The transmitted codewords are shown in the columns on the left, with the ith entry corresponding to the coherent-state complex amplitude on the ith mode. After applying the optical Fourier DT, the codewords are mapped to those on the right. In practice, the transmitted codewords can be generated at the encoder by preparing the output codewords and applying the inverse Fourier DT $U_F^\dagger$.

Now, in order to compute the soft-decoding rate we need to characterize the outcomes via a vector $\mathbf{m}\in[K]_0^{\times L}$, whose ℓth entry counts the number of positions where $\ell=1,\cdots,L$ photons were detected; we define $m=||\mathbf{m}||_1\leqslant K$ as the total number of detection events. For each possible codeword, we also introduce a matrix κ of size $L\times T$, where the row index identifies how many photons were detected, while the column index quantifies which type of pulse produced the given detection event; e.g. $\kappa_{\ell,t}$ is the number of ℓ-photon-detection events due to a t-type pulse. We indicate the ℓth row as $\boldsymbol{\kappa}^\ell$ and the tth column as $\boldsymbol{\kappa}_t$; with this notation, it holds that $||\boldsymbol{\kappa}^\ell||_1=m_\ell$ is the total number of ℓ-photon detection events and $||\boldsymbol{\kappa}_t||_1=k_t\leqslant K_t$ is the total number of t-type pulses that gave rise to a detection event. The conditional probability of observing $\mathbf{m}$ clicks given a $\mathbf{k}$-type codeword then is

$$P(\mathbf{m}|\kappa)=\prod_{\ell=1}^{L}\left(\prod_{t=1}^{T}\mathrm{TP}\left(\ell|n_t,L\right)^{\kappa_{\ell,t}}\right)\cdot\prod_{t=1}^{T}\mathrm{TP}\left(0|n_t,L\right)^{K_t-k_t},\tag{42}$$

where we have defined the truncated Poisson distribution as

$$\mathrm{TP}\left(\ell|\lambda,L\right)=\begin{cases}e^{-\lambda}\frac{\lambda^\ell}{\ell!} & \ell<L,\\ 1-\sum_{\ell=0}^{L-1}\mathrm{TP}\left(\ell|\lambda,L\right) & \ell=L.\end{cases}\tag{43}$$

Furthermore, a given κ is compatible with

$$C(\kappa, L) = \prod_{\ell=1}^{L} \binom{m_\ell}{\boldsymbol{\kappa}^\ell} \cdot \binom{M-m}{K_1 - k_1, \cdots, K_T - k_T, M-K} \tag{44}$$

codewords. Hence, the marginal probability of observing $\mathbf{m}$ clicks in specific positions is

$$\bar{P}(\mathbf{m}) = \frac{1}{\binom{M}{\mathbf{K}, M-K}} \sum_{\kappa \in \mathcal{K}(\mathbf{m})} C(\kappa, L)\, P(\mathbf{m}|\kappa), \tag{45}$$

where

$$\mathcal{K}(\mathbf{m}) = \left\{ \kappa\ L \times T \text{ matrix} : ||\boldsymbol{\kappa}^\ell||_1 = m_\ell\ \forall \ell = 1, \cdots, L,\ ||\boldsymbol{\kappa}_t||_1 \leqslant K_t \forall t = 1, \cdots, T \right\} \tag{46}$$

is the set of all matrices κ compatible with $\mathbf{m}$ clicks of $\mathbf{K}$ types. Finally, note that for a given number of clicks $\mathbf{m}$, there are $\binom{M}{\mathbf{m}, M-m}$ different ways in which they can be distributed among the M positions of the sequence of quantum states transmitted on the channel. Using the fact that

$$C(\kappa) \binom{M}{\mathbf{m}, M-m} = \binom{M}{\mathbf{K}, M-K} \prod_{t=1}^{T} \binom{K_t}{\boldsymbol{\kappa}_t, K_t - k_t}, \tag{47}$$

we can then express the marginal probability as

$$\bar{P}(\mathbf{m}) = \frac{1}{\binom{M}{\mathbf{m}, M-m}} \sum_{\kappa \in \mathcal{K}(\mathbf{m})} \prod_{t=1}^{T} \left[\binom{K_t}{\boldsymbol{\kappa}_t, K_t - k_t} \left(\prod_{\ell=1}^{L} \mathrm{TP}(\ell|n_t, L)^{\kappa_{\ell,t}} \right) \mathrm{TP}(0|n_t, L)^{K_t - k_t} \right] \tag{48}$$

$$= \frac{\Pr(\mathbf{S} = \mathbf{m})}{\binom{M}{\mathbf{m}, M-m}}. \tag{49}$$

Here we identified the distribution of a random variable $\mathbf{S} \in [K]_0^{\times L}$ given by $\mathbf{S} = \sum_{i=1}^{K} \mathbf{Y}_i$, where each $Y_{i,\ell} = \delta_{X_i,\ell}$ for $\ell = 1, \cdots, L$ is a random variable that is non-zero only when the event $X_i = \ell$ takes place. Furthermore, each random variable $X_i \in [L]_0$ corresponds to the result of a $(L+1)$-outcome trial; these variables are divided into T groups of size K_t for $t = 1, \cdots, T$, such that the random variables in group t have the same probability mass function $\mathrm{TP}(\ell|n_t, L)$ for $\ell = 0, \cdots, L$. It is straightforward to see that $\mathbf{Y}_i$ is supported on $L+1$ points and distributed as follows

$$\Pr(\mathbf{Y}_i) = \begin{cases} \Pr(X_i = \ell) & Y_{i,\ell} = 1,\ Y_{i,\ell' \neq \ell} = 0, \\ \Pr(X_i = 0) & \mathbf{Y}_i = 0. \end{cases} \tag{50}$$

Then the probability generating function of $\mathbf{S}$ is simply given by the product of the generating functions of each $\mathbf{Y}_i$:

$$G_{\mathbf{S}}(\mathbf{z}) = \prod_{i=1}^{K} G_{\mathbf{Y}_i}(\mathbf{z}) = \prod_{i=1}^{K} \left(\Pr(X_i = 0) + \sum_{\ell=1}^{L} \Pr(X_i = \ell) \cdot z_\ell \right), \tag{51}$$

where $\mathbf{z} = (z_1, \cdots, z_L)$ is the multi-dimensional argument of the generating function and the corresponding probability mass function can be easily obtained from the coefficients of $G_{\mathbf{S}}(\mathbf{z})$.

The resulting rate then is

$$R_{\mathrm{fm}}(\mathbf{K}, L) = \frac{1}{M} \sum_{\mathbf{m}} \binom{M}{\mathbf{m}, M-m} \cdot \left[h(\bar{P}(\mathbf{m})) - \sum_{\kappa \in \mathcal{K}(\mathbf{m})} \frac{C(\kappa)}{\binom{M}{\mathbf{K}, M-K}} \cdot h(P(\mathbf{m}|\kappa)) \right] \tag{52}$$

$$= \frac{1}{M} \left[-\sum_{\mathbf{m}} \Pr(\mathbf{S} = \mathbf{m}) \log \bar{P}(\mathbf{m}) \right. \tag{53}$$

$$\left. + \sum_{\kappa} \prod_{t=1}^{T} \left[\binom{K_t}{\boldsymbol{\kappa}_t, K_t - k_t} \left(\prod_{\ell=1}^{L} \mathrm{TP}(\ell|n_t, L)^{\kappa_{\ell,t}} \right) \mathrm{TP}(0|n_t, L)^{K_t - k_t} \right] \log P(\mathbf{m}|\kappa) \right] \tag{54}$$

$$= \frac{1}{M} \left[H(\mathbf{S}) + \mathbb{E}_{\mathbf{m} \sim \Pr(\mathbf{S})} \left[\log \binom{M}{\mathbf{m}, M-m} \right] \right. \tag{55}$$

$$+\sum_{t=1}^{T}\mathbb{E}_{\boldsymbol{\kappa}_t\sim\mathrm{Mult}(K_t,\mathrm{TP}(\cdot|n_t,L))}\left[\sum_{\ell=1}^{L}\kappa_{\ell,t}\log\mathrm{TP}\left(\ell|n_t,L\right)+\left(K_t-k_t\right)\log\mathrm{TP}\left(0|n_t,L\right)\right]\Bigg] \tag{56}$$

$$=\frac{1}{M}\left[H(\mathbf{S})+\mathbb{E}_{\mathbf{m}\sim\Pr(\mathbf{S})}\left[\log\binom{M}{\mathbf{m},M-m}\right]-\sum_{t=1}^{T}K_tH\left(\mathrm{TP}\left(\cdot|n_t,L\right)\right)\right] \tag{57}$$

where in the second term of the second equality we have written the sum over $\mathbf{m}$ and $\kappa\in\mathcal{K}(\mathbf{m})$ as an unconstrained sum over all allowed κ values, and in the third one we have observed that $\boldsymbol{\kappa}_t$ follows a multinomial distribution with a success probability $\mathrm{TP}\left(\ell|n_t,L\right)$ for each event $\ell=0,\cdots,L$ and total number of trials K_t. Note that for $T=L=1$ we recover the single-level multi-pulse FM rate (23).

We compare the performance of multi-level FM with a multi-level OOK strategy, where T pulses with probability p_t and mean-photon-number n_t are used, such that $\sum_{t=1}^{T}p_tn_t=n$, while with probability $p_0=1-\sum_{t=1}^{T}p_t$ the vacuum is sent; in the following, we call this a multi-level $(\mathbf{p},\mathbf{n})$-OOK strategy. For a T-pulse protocol, counting up to L photons we obtain a rate

$$R_{\mathrm{ook}}\left(\mathbf{p},\mathbf{n},T\right)=\sum_{\ell=0}^{L}\left[h\left(\delta_{\ell,0}p_0+\sum_{t=1}^{T}p_t\,\mathrm{TP}\left(\ell|n_t,L\right)\right)-\sum_{t=1}^{T}p_t\cdot h\left(\mathrm{TP}\left(\ell|n_t,L\right)\right)\right]. \tag{58}$$

In the small-n limit it holds

$$\mathrm{TP}\left(\ell|n_t,L\right)\simeq\begin{cases}1-\frac{Mn}{TK_t} & \ell=0,\\ \frac{1}{\ell!}\left(\frac{Mn}{TK_t}\right)^{\ell} & 0<\ell\leqslant L,\end{cases} \tag{59}$$

and

$$\Pr\left(\mathbf{S}=\mathbf{m}\right)\simeq\begin{cases}1-Mn & \mathbf{m}=0,\\ Mn & m_1=1,\,m_{\ell>1}=0,\\ 0 & \text{otherwise},\end{cases} \tag{60}$$

i.e. only events where up to 1 photon was counted survive at first order in n. Therefore, we can approximate the multi-level FM rate as

$$R_{\mathrm{fm}}\left(\mathbf{K},L\right)\simeq\frac{1}{M}\left[H_2\left(Mn\right)+Mn\log M-\sum_{t=1}^{T}K_tH_2\left(\frac{Mn}{TK_t}\right)\right] \tag{61}$$

$$\simeq\frac{1}{M}\left[Mn\log M+Mn\log\frac{1}{Mn}-\sum_{t=1}^{T}\frac{Mn}{T}\log\frac{TK_t}{Mn}\right] \tag{62}$$

$$\simeq n\log\frac{M}{T\prod_{t=1}^{T}K_t^{1/T}}. \tag{63}$$

where we used that $H_2(x)\simeq h(x)=x\log\frac{1}{x}$ at $x\simeq0$. Comparing (63) with (25), we observe that one can obtain similar behavior to the single-level case with a multi-level protocol of suitable $\mathbf{K}$, such that its geometric mean is T times smaller than the number of pulses in the single-level protocol. For example, simply choosing $\mathbf{K}_t=K/T$ effectively introduces different pulse types while maintaining the total number of pulses constant. Furthermore, using the AM-GM inequality we have that $\prod_{t=1}^{T}K_t^{1/T}\leqslant\sum_{t=1}^{T}K_t/T$, which implies in this limit

$$R_{\mathrm{fm}}\left(\mathbf{K},L\right)\geqslant R_{\mathrm{fm}}\left(K\right)\ \forall\mathbf{K}:||\mathbf{K}||_1=K, \tag{64}$$

i.e. in the small-n limit the multi-level FM rate cannot be smaller than the single-level FM rate with the same total number of pulses. Let us also note that these small-n rates do not depend on the number of counted photons L, as long as $L\geqslant1$, hence they can be attained with simple threshold photodetectors. Note also that the AM-GM inequality is attained by a vector $\mathbf{K}$ with equal components, implying that the optimal choice of the number of pulses of each type is non-uniform.

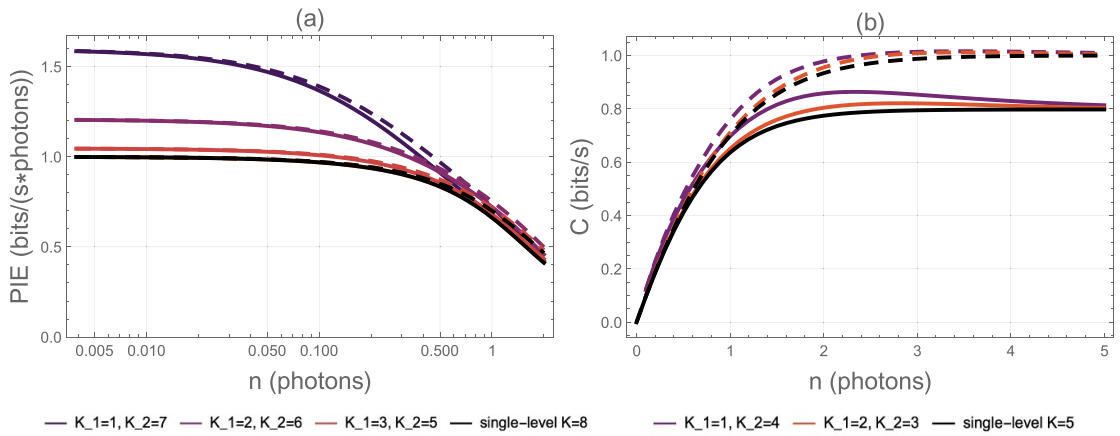

Figure 9. (a) (Solid curves) Plot of the multi-level FM PIE (57) for $M=16$, $T=2$ pulse types and $L=4$; different colors correspond to different numbers of pulses $\mathbf{K}=(K_1,K_2)$ for each type, fixing the total number of pulses to $K=8$; the black curve corresponds to a single-level $K=8$-pulse FM. (dashed lines) Matching $T=2$-pulse OOK PIE (58) for $n_t=n/(Tp_t)$ for all $t=1,2$ and $\mathbf{p}=\mathbf{K}/M$. (b) (solid curves) Plot of the multi-level FM rate (57) for $M=10$, $T=2$ pulse types and $L=4$; different colors correspond to different $\mathbf{K}$ with $K=5$; the black curve corresponds to a single-level $K=5$-pulse FM. (dashed lines) Matching $T=2$-pulse OOK rate (58) for $n_t=n/(Tp_t)$ for all $t=1,2$ and $\mathbf{p}=\mathbf{K}/M$.

Note that, in the same limit, the multi-level OOK rate for $n_t=n/(Tp_t)$ can be written as

$$R_{\rm ook}(\mathbf{p},\mathbf{n},T)\Big|_{n_t=n/(Tp_t)\,\forall t} \simeq h\left(p_0+\sum_{t=1}^{T}p_t\left(1-\frac{n}{Tp_t}\right)\right)-\sum_{t=1}^{T}p_t h\left(1-\frac{n}{Tp_t}\right) \tag{65}$$

$$+h\left(\sum_{t=1}^{T}p_t\frac{n}{Tp_t}\right)-\sum_{t=1}^{T}p_t h\left(\frac{n}{Tp_t}\right) \tag{66}$$

$$\simeq h(n)+\frac{n}{T}\sum_{t=1}^{T}\log\frac{n}{Tp_t}\simeq n\log\frac{1}{T\prod_{t=1}^{T}p_t^{1/T}}, \tag{67}$$

where we used $h(1-x)\simeq -x$ for $x\simeq 0$. In particular, picking also $\mathbf{p}=\mathbf{K}/M$, we have that the corresponding OOK rate is attained at first order in n by the multi-level FM rate:

$$R_{\rm ook}(\mathbf{p},\mathbf{n},T)\Big|_{\substack{\mathbf{p}=\mathbf{K}/M,\\ n_t=n/(Tp_t)\,\forall t}} \simeq n\log\frac{M}{T\prod_{t=1}^{T}K_t^{1/T}}. \tag{68}$$

4.1. Performance analysis in the large-photon-number regime

Similarly, in the large-n limit we have at leading order $\mathrm{TP}(\ell|n_t,L)\simeq\delta_{\ell,L}$, implying $\Pr(\mathbf{S}=\mathbf{m})=\delta_{\mathbf{m},\mathbf{K}}$ and

$$R_{\rm fm}(\mathbf{K},L)=\frac{1}{M}\log\binom{M}{\mathbf{K},M-K}\geqslant R_{\rm fm}(K). \tag{69}$$

Hence, also in this limit it can be seen clearly that increasing the types of pulses while keeping their total number fixed results in an increased rate, i.e. the multi-level FM is superior to the single-level one with the same total number of pulses. Furthermore, at variance with the small-n case, the advantage is present also for a uniform $\mathbf{K}$. In the same limit, the multi-level OOK rate with $n_t=n/(Tp_t)\forall t$, $\mathbf{p}=\mathbf{K}/M$ reads

$$R_{\rm ook}(\mathbf{p},\mathbf{n},T)\Big|_{\substack{\mathbf{p}=\mathbf{K}/M,\\ n_t=n/(Tp_t)\,\forall t}} \simeq H_2(p_0)=H_2\left(\frac{K}{M}\right), \tag{70}$$

matching the single-level OOK expression.

These results are confirmed by numerics in figure 9, where we plot the FM PIE for $T=2$ pulse types, fixing the total number of pulses K and varying the number of pulses of each type. In the small-n region, figure 9(a), we observe that the best rate is obtained for the most uneven pulse-type distribution $\mathbf{K}=(1,7)$ even at finite n. Notice that the FM curves quickly approach their limiting OOK rates, with $\mathbf{n}$ and $\mathbf{p}$ chosen as in (68) as $n<1$. In the large-n region, figure 9(b), we also observe that the most uneven $\mathbf{K}$ distributions are superior, but there remains a gap with the corresponding OOK limit.

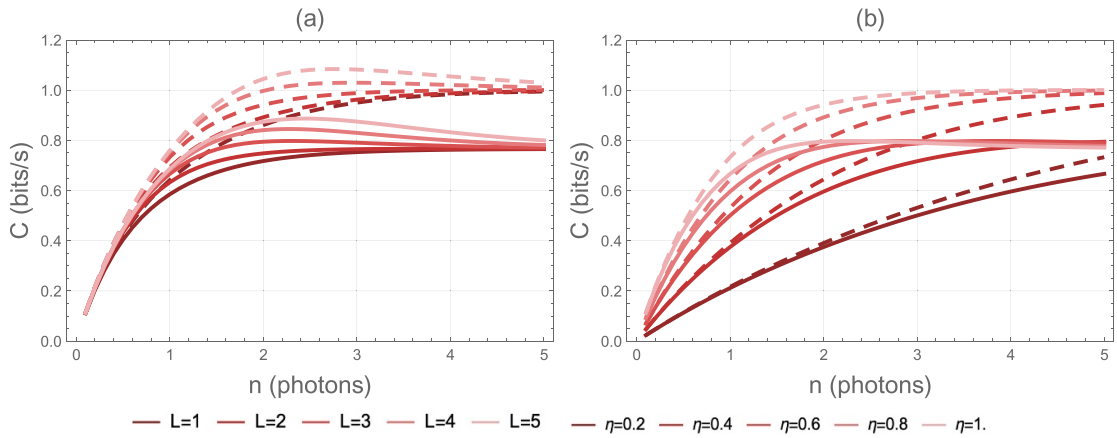

Figure 10. (a): (solid lines) Plot of the multi-level FM rate (57) for $M = 8$, $T = 2$, $\mathbf{K} = (1, 3)$ and varying photon-number resolution L; (dashed lines) Corresponding multi-level OOK rates $n_t = n/(Tp_t)$ for all $t = 1, 2$ and $\mathbf{p} = \mathbf{K}/M$. (b): (solid lines) Plot of the multi-level FM rate (57) for $M = 8$, $T = 2$, $\mathbf{K} = (1, 3)$, $L = 3$ and varying the photo-detection efficiency η; (dashed lines) Corresponding multi-level OOK rates $n_t = n/(Tp_t)$ for all $t = 1, 2$ and $\mathbf{p} = \mathbf{K}/M$.

4.2. Impact of imperfect photon-counting detection

Finally, since we have shown that multi-level codes require the use of photon-counting detectors to fully take advantage of the code structures, here we study the impact of typical limiting factors in such devices: finite photo-detection resolution and efficiency.

In figure 10(a) we study the effect of finite photo-detector resolution L, plotting the $T = 2$-level FM rate for fixed M, $\mathbf{K}$ and varying L. We observe that small values of L have a significant impact on the rate performance of a multi-level FM protocol: increasing the photo-detector resolution L gives rise to a marked increase in the rate, even when $L > K = 4$, i.e. when we are able to distinguish more photon number than there are pulses. It is also clear from the plot that larger values of L are necessary to maintain a large rate as n increases.

In figure 10(b) we study the effect of finite photo-detector efficiency η, which can be obtained from (57) and (58) by rescaling the photon-number of each pulse-type n_t as ηn_t, which effectively changes the mean of the truncated-Poisson distribution. We then plot the $T = 2$-level FM rate for fixed M, $\mathbf{K}$, L and varying η. We observe that values of $\eta < 0.8$ have a significant impact on the rate performance of both the multi-level FM protocol and its OOK counterpart, making the performance of these two schemes approximately similar as η decreases.

5. Conclusions

In this article we introduced generalization of single-pulse JDR's based on the Fourier transform and the use of multiple pulses (multi-pulse FM) and multiple pulse types (multi-level FM). We computed the information-transmission rate attainable with these new code families, showing that they allow to approach the rate of generalized-OOK strategies. The main takeaways are that: (i) using a multi-pulse FM it is possible to use a single Fourier-transform device of fixed order M for a wide range of signal photon-number values, at variance with the single-pulse case; (ii) using a multi-level FM it is possible to study joint-detection at larger photon-numbers, where the introduction of multiple pulse types can surpass the performance of protocols based on binary modulation.

In light of these reasons, we believe that our results on multi-pulse codes will simplify the design of JDR-assisted protocols in the photon-starved regime, facilitating their practical implementation. Further studies might also focus on the application of multi-level codes in the presence of phase-noise, where OOK based on squeezed states is known to provide an advantage with respect to classical coherent-state strategies.

Data availability statement

All data that support the findings of this study are included within the article (and any supplementary files).

Acknowledgments

M R acknowledges support from the Project PNRR—Finanziato dall'Unione europea—MISSIONE 4 COMPONENTE 2 INVESTIMENTO 1.2—'Finanziamento di progetti presentati da giovani ricercatori'—Id MSCA_0000011-SQUID—CUP F83C22002390007 (Young Researchers)—Finanziato dall'Unione europea—NextGenerationEU.

ORCID iD

Matteo Rosati https://orcid.org/0000-0002-8972-2936

References

[1] Holevo A S 1998 Coding theorems for quantum communication channels *IEEE Int. Symp. Inf. Theory - Proc.* p 84
[2] Giovannetti V, García-Patrón R, Cerf N J and Holevo A S 2014 Ultimate classical communication rates of quantum optical channels *Nat. Photon.* **8** 796–800
[3] Mari A, Giovannetti V and Holevo A S 2014 Quantum state majorization at the output of bosonic Gaussian channels *Nat. Commun.* **5** 3826
[4] Hausladen P, Jozsa R, Schumacher B, Westmoreland M and Wootters W K 1996 Classical information capacity of a quantum channel *Phys. Rev.* A **54** 1869–76
[5] Schumacher B and Westmoreland M D 1997 Sending classical information via noisy quantum channels *Phys. Rev.* A **56** 131–8
[6] Giovannetti V, Lloyd S and Maccone L 2012 Achieving the Holevo bound via sequential measurements *Phys. Rev.* A **85** 012302
[7] Wilde M M and Guha S 2013 Polar codes for classical-quantum channels *IEEE Trans. Inf. Theory* **59** 1175–87
[8] Takeoka M, Krovi H and Guha S 2013 Achieving the Holevo capacity of a pure state classical-quantum channel via unambiguous state discrimination *2013 IEEE Int. Symp. Inf. Theory* (IEEE) pp 166–70
[9] Rosati M and Giovannetti V 2016 Achieving the Holevo bound via a bisection decoding protocol *J. Math. Phys.* **57** 062204
[10] Rosati M, Mari A and Giovannetti V 2017 Capacity of coherent-state adaptive decoders with interferometry and single-mode detectors *Phys. Rev.* A **96** 012317
[11] Rosati M, De Palma G, Mari A and Giovannetti V 2017 Optimal quantum state discrimination via nested binary measurements *Phys. Rev.* A **95** 1–10
[12] Garcia Diaz M, Desef B, Rosati M, Egloff D, Calsamiglia J, Smirne A, Skotiniotis M and Huelga Susana F 2020 Accessible coherence in open quantum system dynamics *Quantum* **4** 249
[13] Rosati M 2021 Performance of coherent frequency-shift keying for classical communication on quantum channels *2021 IEEE Int. Symp. Inf. Theory* (IEEE) pp 902–5
[14] Holevo A S 2021 Accessible information of a general quantum Gaussian ensemble
[15] Mishra H K, Lami L, Mandayam P and Wilde M M 2023 Pretty good measurement for bosonic Gaussian ensembles
[16] Rosati M and Solana A 2024 Joint-detection learning for optical communication at the quantum limit *Opt. Quantum* **2** 390
[17] Guha S 2011 Structured optical receivers to attain superadditive capacity and the Holevo Limit *Phys. Rev. Lett.* **106** 240502
[18] Rosati M, Mari A and Giovannetti V 2016 Multiphase Hadamard receivers for classical communication on lossy bosonic channels *Phys. Rev.* A **94** 062325
[19] Cui C, Postlewaite J, Saif B N, Fan L and Guha S 2023 Superadditive Communications with the Green Machine: A Practical Demonstration of Nonlocality without Entanglement
[20] Rosati M and Cincotti G 2024 Optical communications at the quantum limit *2024 24th Int. Conf. Transparent Opt. Networks* (IEEE) pp 1–4
[21] Martinez A 2007 Spectral efficiency of optical direct detection *J. Opt. Soc. Am.* B **24** 739
[22] Cheraghchi M and Ribeiro J 2019 Improved upper bounds and structural results on the capacity of the discrete-time Poisson channel *IEEE Trans. Inf. Theory* vol 65 (Institute of Electrical and Electronics Engineers Inc) pp 4052–68
[23] Fanizza M, Rosati M, Skotiniotis M, Calsamiglia J and Giovannetti V 2021 Squeezing-enhanced communication without a phase reference *Quantum* **5** 608
[24] Fanizza M, Rosati M, Skotiniotis M, Calsamiglia J and Giovannetti V 2020 Performance of Gaussian encodings for classical communication on correlated quantum phase-noise channels *2020 IEEE Int. Symp. Inf. Theory* (IEEE) pp 1830–4
[25] Banaszek K, Kunz L, Jachura M and Jarzyna M 2020 Quantum limits in optical communications *J. Light. Technol.* **38** 2741–54
[26] Nötzel J and Rosati M 2023 Operating fiber networks in the quantum limit *J. Light. Technol.* **41** 6865–74
[27] Dolinar S J 1973 Communication and sciences engineering *Q. Prog. Rep. Research Lab. Electron.* **111** 115
[28] Helstrom C W 1976 *Quantum Detection and Estimation Theory* vol 84 (Academic)
[29] Becerra F E, Fan J and Migdall A 2013 Implementation of generalized quantum measurements for unambiguous discrimination of multiple non-orthogonal coherent states *Nat. Commun.* **4** 2028
[30] Barak R and Ben-Aryeh Y 2007 Quantum fast Fourier transform and quantum computation by linear optics *J. Opt. Soc. Am.* B **24** 231
[31] Reck M, Zeilinger A, Bernstein H J and Bertani P 1994 Experimental realization of any discrete unitary operator *Phys. Rev. Lett.* **73** 58–61
[32] Clements W R, Humphreys P C, Metcalf B J, Steven Kolthammer W and Walsmley I A 2016 Optimal design for universal multiport interferometers *Optica* **3** 1460
[33] Crespi A, Osellame R, Ramponi R, Bentivegna M, Flamini F, Spagnolo N'o, Viggianiello N, Innocenti L, Mataloni P and Sciarrino F 2016 Suppression law of quantum states in a 3D photonic fast Fourier transform chip *Nat. Commun.* **7** 10469